Journal of Power Sources 194 (2009) 774–785

Contents lists available at ScienceDirect

Journal of Power Sources

journal homepage: www.elsevier.com/locate/jpowsour

Thermodynamic analysis of gasification-driven direct carbon fuel cells

Andrew C. Lee[a,*], Reginald E. Mitchell[a], Turgut M. Gür[b,c]

[a] Department of Mechanical Engineering, Stanford University, 452 Escondido Mall, Building 520, Stanford, CA 94305, USA
[b] Department of Materials Science and Engineering, Stanford University, 496 Lomita Mall, Durand Building, Stanford, CA 94305, USA
[c] Direct Carbon Technologies, LLC, Palo Alto, CA 94301 USA

ARTICLE INFO

Article history:
Received 22 April 2009
Received in revised form 21 May 2009
Accepted 22 May 2009
Available online 30 May 2009

Keywords:
Direct carbon fuel cell
Coal
Electricity generation
Gasification
Exergy

ABSTRACT

The gasification-driven direct carbon fuel cell (GD-DCFC) system is compared with systems using separate gasification steps prior to work extraction, under autothermal or indirect constraints. Using simple system exergy analysis, the maximum work output of the indirect gasification scheme is 4–7% lower than the unconstrained direct approach, while the work output of the autothermal gasification approach is 12–13% lower than the unconstrained case. A more detailed calculation for the DCFC and indirect gasification plants, using common solid fuel compositions, gives conversion efficiencies in the range of 51–58% at an operating voltage of 0.7 V selected for both systems in this study. In contrast, the conversion efficiency of the autothermal gasification approach is estimated to be 33–35% at 0.7 V. DCFC efficiencies can be increased to over 60% by an increase in operating voltage and/or inclusion of a bottoming cycle. The thermodynamic model also indicates that steam gasification yields similar work output and thermal efficiency as for CO_2 gasification. Open circuit potential measurements agree with equilibrium calculations both for the C–O and C–H–O gasification systems, confirming the governing mechanism and feasibility of the GD-DCFC. Current–voltage measurements on an un-optimized system demonstrate power densities of 220 mW cm^{-2} at 0.68 V during operation at 1178 K.

1. Introduction

Currently, half of the electricity produced in the United States comes from coal fired power plants. Coal's share of electricity production in many developing countries exceed this amount reaching over 70% in China and India. Given coal's abundance and low price, it is expected that this naturally occurring solid fuel will continue to be relevant to the world's energy portfolio for decades to come.

Historically, pulverized coal has been burned in air to produce sensible enthalpy that is transferred as heat to a Rankine steam cycle equipped with a generator to produce electrical work. This approach has several important drawbacks. Primarily, the conversion efficiencies are in the low 30% range, which are limited by the relatively low temperature steam cycle, and the exhaust stream is highly diluted by N_2 originating from the combustion air and hence, is not ready for CO_2 capture.

Driven by global warming concerns, particularly in regards to CO_2 emissions, emerging coal utilization strategies prevent addition of N_2 into the fuel stream by using pure oxygen from an air separation unit (ASU), thus producing a concentrated CO_2 stream for geological sequestration [1]. Modern efforts to address these concerns have led to more advanced processes like Integrated Gasification Combined Cycle (IGCC) plants, where coal is gasified with steam and oxygen to a syngas that is subsequently cleaned of sulfur and other impurities before utilization in a cascaded, combined gas-steam cycle. This approach does not introduce nitrogen gas into the process stream, and thus the exhaust is more readily suitable for sequestration of CO_2. With IGCC, the higher temperature operation regime of the gas turbine allows higher thermal efficiencies than that of the standalone Rankine cycle. The syngas can also be converted electrochemically via solid oxide fuel cell, similar to the FutureGen program [2,3].

Although long and rich in history [4], direct carbon fuel cells (DCFCs) have recently gained renewed interest as an area of active research and development, encompassing a variety of fuel cell configurations and approaches [5]. All of these approaches share an end goal of eventually converting practical and economically feasible carbonaceous solids (coal, biomass, municipal solid waste, char, etc.) electrochemically to electric power with efficiencies higher than contemporary arrangements, producing an effluent stream of concentrated CO_2.

High temperature, solid oxide fuel cells (SOFCs) based on oxide-ion conducting membranes have garnered widespread attention in the last several decades due to inherent high system efficiencies. Inspired by their compatibility and fuel flexibility, SOFC based

* Corresponding author. Tel.: +1 510 304 9211; fax: +1 650 723 0335.
E-mail addresses: aclee@stanford.edu (A.C. Lee), remitche@stanford.edu (R.E. Mitchell), turgut@stanford.edu (T.M. Gür).

0378-7753/$ – see front matter © 2009 Elsevier B.V. All rights reserved.
doi:10.1016/j.jpowsour.2009.05.039

Nomenclature

a, b, c, d	molar coefficients
C_P	specific heat ($J\,mol^{-1}\,K^{-1}$)
E	electric potential (V)
F	Faraday's constant ($C\,equiv.^{-1}$)
g	specific Gibbs free energy ($J\,mol^{-1}$)
h	specific enthalpy ($J\,mol^{-1}$)
Δh_f	heat of formation ($J\,mol^{-1}$)
$\dot{H}$	stream enthalpy ($MJ\,s^{-1}$)
HV	heating value ($J\,mol^{-1}$)
$\dot{HV}$	stream heating value ($MJ\,s^{-1}$)
HHV	higher heating value ($MJ\,kg^{-1}$)
I	current (A)
$\dot{m}$	mass flow ($kg\,s^{-1}$)
MW	molecular mass ($kg\,mol^{-1}$)
n	number of stoichiometric electrons
N	number of species
$\dot{N}$	molar flow ($mol\,s^{-1}$)
P	pressure (atm)
q	specific energy transfer as heat ($J\,mol^{-1}$)
$\dot{Q}$	energy transfer as heat ($MJ\,s^{-1}$)
R_u	universal gas constant ($J\,mol^{-1}\,K^{-1}$)
s	specific entropy, ($J\,mol^{-1}\,K^{-1}$)
$\dot{S}_{gen}$	entropy generation ($MJ\,s^{-1}\,K^{-1}$)
T	temperature (K)
U_a	air utilization
U_f	fuel utilization
w	specific work ($J\,mol^{-1}$)
$\dot{W}$	work transfer ($MJ\,s^{-1}$)

Greek letters

ε	heat exchanger effectiveness
η	efficiency
σ	entropy generation ($J\,mol^{-1}\,K^{-1}$)
$\dot{\Psi}$	stream exergy ($MJ\,s^{-1}$)

Subscripts

0	reference state
a	ash
B	bottoming cycle
c	carbon
C	indicator of cold stream
cell	cell operating property
fuel	fuel property
gas	gasification process
h	hydrogen
H	indicator of hot stream
i	index for species
in	transfer into system
O	oxygen
$O_{2,a}$	oxygen at the SOFC anode
$O_{2,c}$	oxygen at the SOFC cathode
OCV	open circuit voltage
out	transfer out of system
p	product of a reactor
r	reactant of a reactor
SOFC	solid oxide fuel cell
stream	stream property

DCFC systems have been investigated by several groups. Nakagawa and Ishida evaluated the performance of a SOFC driven by gasification of 4 mm charcoal particles without anode-side gas flow [6]. Coupled with their experimental evaluation is an exergy analysis, showing the irreversibilities associated with chemical reaction, ohmic loss and electrode polarization. One major finding was that higher temperature operation (1275 K opposed to 1075 K) reduced exergy losses due to faster kinetics and decreased ohmic resistance. That study also mentioned the possibility of using the heating value of the flue gas to provide heat for the SOFC. Similarly, Gür and Huggins [7] have reported typical fuel cell behavior and power generation from a fixed bed of carbon physically detached from the anode surface of a tubular SOFC element. Wang et al. used a similar configuration, with CO_2 flowing through a physically separate coal gasifier, and syngas directed to a tubular mixed ionically and electronically conducting membrane, rather than SOFC, without gas cleanup [8]. The sensible heat release from reaction with the diffusing oxygen could then be used to drive a heat engine or other process. This arrangement has practical interest in eliminating cryogenic oxygen separation units. Horita et al. [9] employed a graphitic anode, pressed into a bed of graphite and metal carbide particles, with Ar or CO_2 flowing through the fixed bed. Hasegawa and Ihara [10,11] reported battery type behavior while studying possible reaction mechanisms of carbon deposited on solid anodes from the gas phase. Recently, solid fuel conversion and electrical power generation have been reported in a FB-DCFC physically coupled to a minimally fluidized bed of carbonaceous solid fuels in direct contact with the anode surface [12,13]. These approaches all give open circuit voltages (OCV) of about 0.8–0.9 V with CO_2 flowing through the system, or about 1.1–1.2 V with no gas flow or an inert purge.

There are other DCFC configurations pursued for direct conversion of solid fuels. Systems based on molten carbonate fuel cell (MCFC) arrangements [14] or hybrid SOFC–MCFC arrangements [15] have been investigated. Hemmes et al. [16] performed a thermodynamic analysis of a molten carbonate DCFC operating at 800 °C on pure carbon, calculating thermal efficiencies reaching 78%. Cooper also reported thermal efficiencies ranging from 70 to 80% for MCFC based systems [17]. Efficiencies of 60–85%, based on cell potential, were reported by Zecevic et al., and an estimate of 70–75% was made for practical DCFC efficiencies based on systems with molten hydroxide electrolytes [18]. Tao reported efficiencies of 60–70% for an SOFC assembly with molten Sn anode [19]. In all these DCFC arrangements, the solid fuel is dispersed in the molten anode medium sometimes exceeding the percolation limit in order to assure the electrical connectivity and contiguity of the anode.

The DCFC examined here offers the advantage of a thermally integrated, all-solid-state electrochemical system, with established pulverized fuel delivery and infrastructure as well as ash separation mechanisms. One inherent requirement with DCFC systems is that the anode and electrolyte be chemically resilient to the fuel used. In practical terms, this means that the fuel cell components must be tolerant of sulfur, ash, condensable hydrocarbons and other minor species, or alternatively there exists an in situ capture mechanism, or thirdly that the fuel be processed to remove such species prior to use.

In the present study, the solid state, single-step DCFC is considered for comparative analysis with autothermal and indirect gasification systems, although the results apply to any DCFC system in which solid fuel gasification occurs in situ within the anode chamber and dominates the fuel cell performance. A thermodynamic analysis is performed for carbon, showing that separate gasification processes (autothermal or indirect) produce irreversibilities due to imposed constraints, thus lowering the work producing ability of the system, regardless of the nature of the work producer. Following this analysis, more detailed systems employing a solid oxide based fuel cell are investigated to further support the DCFC process relative to separate gasification.

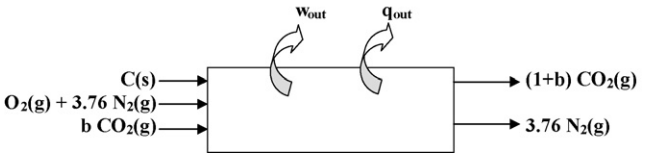

Fig. 1. Schematic representation of a single-step system that extracts work from carbon, with an unmixed CO_2 exhaust stream.

2. General thermodynamic considerations on systems level

2.1. Carbon work potential with direct conversion

The potential for producing useful work (w_{out}) from a fuel is dependent upon the specified thermochemical states of the fuel, oxidizer and products, the environmental state, and any constraints imposed on the system, such as operating temperature or mixing amongst the inlet streams or amongst the outlet streams. The maximum useful work is produced when the system operates reversibly. A simple control volume, as shown in Fig. 1, can be used to determine the steady, work-producing potential of converting the solid, graphitic carbon at 298 K along with gaseous CO_2 at 298 K and environmental air at 298 K and 1 atm into gaseous CO_2 and N_2 at the environmental dead state of 298 K and 1 atm. The exhaust CO_2 and N_2 streams are constrained to be unmixed, indicative of a system with capture ready CO_2. The heat interaction (q_{out}) is taken to occur at the environmental temperature, which is not the case for real work producers. Note that the specific means of work production is not defined nor required during exergy analysis. Inclusion of a real work producer, such as a fuel cell or heat engine, would introduce additional constraints, which will be considered in the following sections.

The mole-specific enthalpy (h_i), entropy (s_i), and Gibbs function (g_i) of species i in streams entering and exiting the control volume are calculated via Eqs. (1)–(3), respectively, assuming gases and solids behave ideally, with solids having unit activity. The reference pressure is taken to equal the environmental pressure (P_0) of 1 atm. The 1st and 2nd laws of thermodynamics applied to the control volume are given by Eqs. (4) and (5), respectively. The enthalpy of formation ($\Delta h_{f,i}$) is maintained in the species enthalpy to account for chemical change. The maximum work is achieved when the entropy generation (σ) is identically zero, i.e. when the system operates reversibly. By using this fact, and combining the 1st and 2nd laws, an expression for the work output (per mole carbon) results, as given by Eq. (6):

$$h_i(T) = \Delta h_{f,i}(298\,\mathrm{K}) + \int_{298\,\mathrm{K}}^{T} C_P(T')\,dT' \tag{1}$$

$$s_i(T, P_i) = s_i(T, P_0) - R_u \ln\left(\frac{P_i}{P_0}\right) \tag{2}$$

$$g_i(T, P_i) = h_i(T) - Ts_i(T, P_i) \tag{3}$$

$$0 = w_{out} + q_{out} + (1+b)h_{CO_2}(T_0) - h_C(T_0) - h_{O_2}(T_0) - bh_{CO_2}(T_0) \tag{4}$$

$$\sigma = \frac{q_{out}}{T_0} + s_{CO_2}(T_0, P_0) + 3.76(s_{N_2}(T_0, P_0) - s_{N_2}(T_0, 0.79P_0)) - s_C(T_0) - s_{O_2}((T_0, 0.21P_0)) \tag{5}$$

$$w_{out} = [g_C(T_0) + g_{O_2}(T_0, 0.21P_0) + 3.76g_{N_2}(T_0, 0.79P_0) - g_{CO_2}(T_0, P_0) - 3.76g_{N_2}(T_0, P_0)] - T_0\sigma \tag{6}$$

Evaluating Eq. (6), using thermochemical data tabulated in the NIST-JANAF tables [20], yields a value of 388.3 kJ mol_C^{-1} for the maximum work output (which can be compared to 394.4 kJ mol_C^{-1} if P_{O_2} were 1 atm and no N_2 were present). The exergy differs from the heating value of carbon (393.5 kJ mol_C^{-1}) by only about 1%. Not that the work output is not dependent upon the input CO_2 stream, since this stream enters and leaves the control volume at the same condition, hence its inclusion is arbitrary.

This schematic also nearly represents the ideal DCFC configuration, where oxygen, carbon, and possibly carbon dioxide are brought into the system, and carbon dioxide leaves at T_0 and P_0. Implicit assumptions include chemical equilibrium in the gasifier, a completely reversible fuel cell, full carbon conversion to CO_2, and an effluent stream of pure CO_2 at 298 K. In practical terms, any bottoming cycle or use of actual DCFC heat rejection is included in this work value. In an actual system, the 298 K reactants are heated to some gasification temperature and the hot products are then cooled back to 298 K either by bottoming cycle or irreversible heat rejection to the environment. These irreversibilities will necessarily lower the actual, useful work that can be delivered by such devices.

2.2. Carbon work potential with indirect gasification

The previous calculation is now repeated for a system in which solid carbon is gasified indirectly in control volume I, and then undergoes a work extraction process in control volume II, as shown in Fig. 2. Indirect gasification here refers to gasification with CO_2 (or H_2O) and sensible heat addition ($q_{in,gas}$), but no gaseous oxygen addition.

The output of the gasifier is constrained to be in equilibrium at temperature T_{gas}, which is imposed by kinetic considerations, and a total pressure of 1 atm. The equilibrium mole fraction of O_2 exiting the gasifier is of the order of 1e−20, and is neglected for simplicity. No work interaction is allowed for control volume I (gasifier). The input CO_2 molar coefficient "b" is uniquely determined to give the maximum CO/CO_2 ratio exiting the gasifier without solid carbon present. The molar coefficients "c" and "d" are uniquely determined from the equilibrium composition. The 1st and 2nd laws of thermodynamics can again be written, for each control volume, and algebraically combined to determine the work output. The result, given in Eq. (7), is identical to the unconstrained case except for the

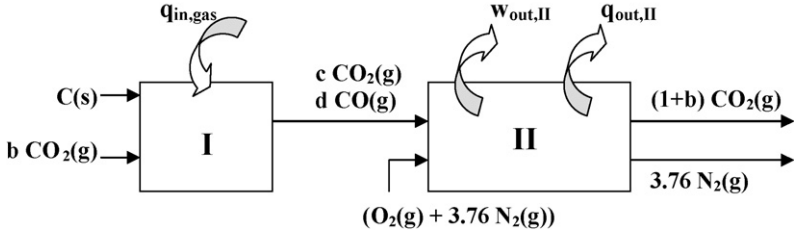

Fig. 2. Schematic representation of a two-step system that extracts work from carbon that includes an indirect gasification step.

irreversibility of the gasification step. This work output is a maximum when system defined by control volume II operates reversibly, and entropy generation σ_{II} as given by Eq. (8) is identically zero. The entropy generation of control volume I, due to chemical reaction and heat transfer across a finite temperature difference, is calculated by evaluating Eq. (9):

$$w_{out,II} = [g_C(T_0) + g_{O_2}(T_0, 0.21P_0) + 3.76g_{N_2}(T_0, 0.79P_0) - g_{CO_2}(T_0, P_0) - 3.76g_{N_2}(T_0, P_0)] - T_0(\sigma_I + \sigma_{II}) \quad (7)$$

$$\sigma_{II} = \frac{q_{out,II}}{T_0} + (1+b)s_{CO_2}(T_0, P_0) + 3.76(s_{N_2}(T_0, P_0) - s_{N_2}(T_0, 0.79P_0)) - cs_{CO}(T_{gas}, P_{CO,gas}) - ds_{CO_2}(T_{gas}, P_{CO,gas}) - s_{O_2}(T_0, 0.21P_0) \quad (8)$$

$$\sigma_I = cs_{CO}(T_{gas}, P_{CO,gas}) + ds_{CO_2}(T_{gas}, P_{CO_2,gas}) - s_C(T_0) - bs_{CO_2}(T_0, P_0) - \frac{q_{in,gas}}{T_{gas}} \quad (9)$$

The maximum work outputs for indirect gasification at T_{gas} values of 1073, 1173, and 1273 K are 370.1, 367.5, and 363.6 kJ mol_C^{-1} respectively. This corresponds to a 4–7% reduction in work output from the unconstrained case. The work potentials of the heat input q_{gas} at temperatures of 1073, 1173, and 1273 K are 166, 171, and 180 kJ mol_C^{-1}, respectively, giving 2nd law efficiencies for the IDG plant of 67, 66, and 64%, compared to the unconstrained case. Although the work output per carbon input is only slightly lower than the unconstrained case, the efficiency has been significantly reduced due to the additional heat input. If the heat input for gasification can be provided by heat rejection from process II, then the input can be reduced and efficiency can be increased. Heat transfer from sources at temperatures higher than T_{gas} will have a higher corresponding irreversibility.

2.3. Carbon work potential with autothermal gasification

The previous work calculation is now repeated for a system in which solid carbon is gasified autothermally in control volume I, and then undergoes an ideal reversible work extraction process in control volume II, as shown in Fig. 3. Autothermal gasification refers to gasification with gaseous oxygen and modifier (H_2O or CO_2) such that the system is adiabatic. For simplicity, only results for CO_2 are included. All streams again have a total pressure of 1 atm. The first control volume (gasifier) is adiabatically constrained and without work interaction. In addition, the gasifier C/O ratio is maximized, under the constraint that there is no solid carbon present in the gasified equilibrium products. Again, the trace O_2 exiting the gasifier is neglected for simplicity. The CO/CO_2 stream leaving the gasifier is at a specified gasification temperature T_{gas}. The four gasification constraints (carbon balance, oxygen balance, energy balance and equilibrium ratio) exactly define the molar coefficients *a*, *b*, *c*, and *d*. Air, at 298 K, is then introduced with the gasification products into the second control volume, which allows for work and heat interactions. The separate N_2 streams leaving both control volumes are constrained to 298 K and 1 atm total pressure.

The work output $w_{out,II}$, after algebraic combination, is shown in Eq. (10), and is a maximum when σ_{II}, given by Eq. (11), is identically zero. The entropy produced by the gasification control volume is given by Eq. (12):

$$w_{out,II} = [g_C(T_0) + g_{O_2}(T_0, 0.21P_0) + 3.76g_{N_2}(T_0, 0.79P_0) - g_{CO_2}(T_0, P_0) - 3.76g_{N_2}(T_0, P_0)] - T_0(\sigma_I + \sigma_{II}) \quad (10)$$

$$\sigma_{II} = \frac{q_{out,II}}{T_0} + (1+b)s_{CO_2}(T_0, P_0) + 3.76(1-a)(s_{N_2}(T_0, P_0) - s_{N_2}(T_0, 0.79P_0)) - cs_{CO}(T_{gas}, P_{CO,gas}) - ds_{CO_2}(T_{gas}, P_{CO,gas}) - (1-a)s_{O_2}(T_0, 0.21P_0) \quad (11)$$

$$\sigma_I = cs_{CO}(T_{gas}, P_{CO,gas}) + ds_{CO_2}(T_{gas}, P_{CO_2,gas}) + 3.76a(s_{N_2}(T_0, P_0) - s_{N_2}(T_0, 0.79P_0)) - s_C(T_0) - as_{O_2}(0.21P_0) - bs_{CO_2}(T_0, P_0) \quad (12)$$

The resulting form of Eq. (10) is almost identical to Eqs. (6) and (7), with identical input and output streams, except that the irreversibility of the gasification step has changed. Since the input and output states, and the work and heat interactions are specified for the gasifier, the irreversibility of the gasifier is now uniquely set. Control volume II has specified input and output states, but the heat and work interactions are not specified. At gasification temperatures of 1073, 1173, and 1273 K, the maximum work outputs ($\sigma_{II} = 0$) are 338.4, 340.2 and 340.4 kJ mol_C^{-1} respectively, or 12–13% less than the unconstrained approach shown in Fig. 1. The work output of the system shown in Fig. 3 is less than 388.3 kJ mol_C^{-1} due to the irreversible chemical gasification process, with 2nd law efficiencies of 87% for all three temperatures. Since no work is extracted during gasification, none of the potential work is realized.

This general analysis shows clearly that constraints lead to lower work potentials, and that the reversible introduction of oxygen from air allows for higher work potentials. The approaches using separate gasification steps are shown to incur higher losses than the arrangement without separate gasification.

2.4. Work potential of a carbon fuel cell

Thermodynamically, separate gasification processes can introduce lost work potential. The GD-DCFC approach requires that solids gasification and work output occur from the same reactor, although not necessarily during the same chemical process. Regardless of whether in situ carbon gasification to CO drives the fuel cell, or solid carbon participates directly in the electrochemical reaction, four electrons are required for full conversion of a carbon atom to carbon dioxide. Reactions (R1) and (R2) show the two-step global progression of one mole of solid carbon to CO_2. The key point asserted here is that oxygen not initially bound in CO_2 can only enter the system via the electrolyte, thus producing work.

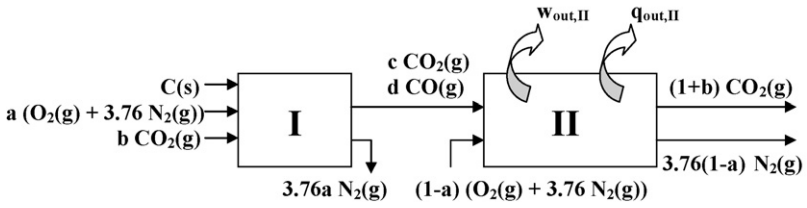

Fig. 3. Schematic representation of a two-step system that extracts work from carbon that includes an autothermal gasification step.

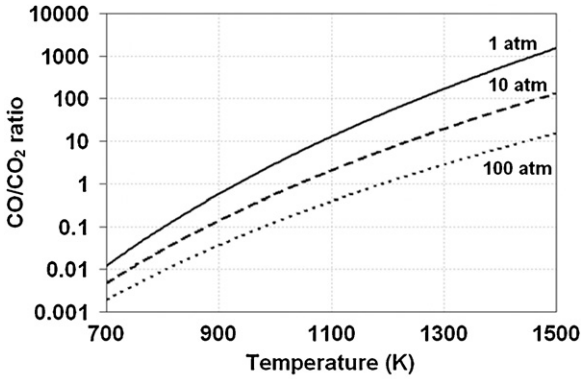

Fig. 4. Calculated CO/CO_2 mole ratio for Boudouard equilibrium at various total pressures.

Reaction:

$$C + CO_2 \rightarrow 2CO \quad (R1)$$

$$2CO + 2O^{2-} \rightarrow 2CO_2 + 4e^- \quad (R2)$$

In essence, the GD-DCFC uses the SOFC to both gasify the carbon and convert the gasification products to CO_2. This necessitates that solids will be in contact with the anode. Displayed in Fig. 4 is the CO/CO_2 ratio for Boudouard equilibrium, while displayed in Fig. 5 is the theoretical open circuit potential for relevant electrochemical interactions at a total pressure of 1 atm. Open circuit potentials were calculated using the Nernst equation (see Eq. (13)), with $n = 4$, $P_{O_2,c}$ equal to 0.21, and $P_{O_2,a}$ determined by the anode-side composition. In accord with the Le Chatelier principle, higher pressure suppresses Reaction (R1) towards CO_2:

$$E_{OCV} = \frac{R_u T}{nF} \ln\left(\frac{P_{O_2,c}}{P_{O_2,a}}\right) \quad (13)$$

Pressurization of the anode compartment is not preferred thermodynamically, as the Nernst equation gives a decreased OCV with higher anode pressure. A reduction in OCV also occurs if both the anode and cathode are pressurized equally, due to the decreased equilibrium CO/CO_2 ratio as demonstrated in Fig. 4. Pressurization of the cathode side alone would increase the OCV, but also create a large pressure differential across the electrode–electrolyte assembly. High pressure operation has been shown, however, to increase gasification reaction rates [21]. Increased reaction rates allow for smaller reaction vessels, smaller residence times, and larger power densities. This study only addresses the thermodynamic aspects of the DCFC system, and thus reaction rates are not resolved.

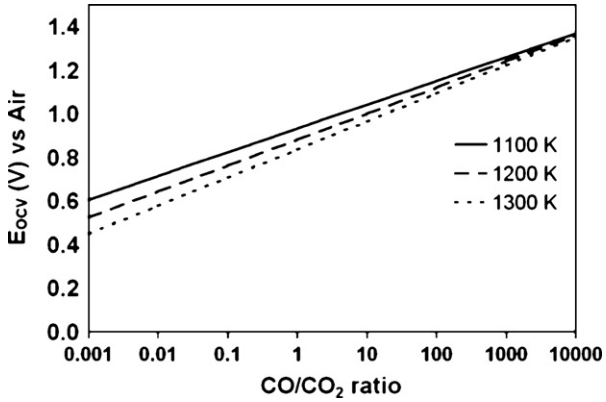

Fig. 5. Open circuit voltage for $CO + 0.5O_2 \leftrightarrow CO_2$ at 1 atm total pressure, for various CO/CO_2 ratios at the anode and cell temperatures.

There are several carbon and hydrogen containing reactions that represent global electrochemical reactions, as given by Reactions (R3)–(R6).

Reaction:

$$C + O_2 \rightarrow CO_2 \quad (R3)$$

$$C + 0.5O_2 \rightarrow CO \quad (R4)$$

$$CO + 0.5O_2 \rightarrow CO_2 \quad (R5)$$

$$H_2 + 0.5O_2 \rightarrow H_2O \quad (R6)$$

If the anode side gas environment is not in Boudouard equilibrium, then the CO/CO_2 ratio depends upon the finite rates of chemical and/or transport processes. Shown in Fig. 5 is the open circuit potential variation with CO/CO_2 ratio and temperature, at a total pressure of 1 atm for Reaction (R5). The OCV is significantly affected by the CO/CO_2 ratio. Experimental data of 0.8–0.9 V near 900 C is indicative of CO/CO_2 ratios near order of one. This is caused by introduction of CO_2 into the carbon bed and the finite rate of the Boudouard reaction producing CO [22]. If an inert species purges the anode gaseous environment, the trace CO and CO_2 will skew towards equilibrium values in the presence of carbon giving OCV values over 1 V. If the CO/CO_2 ratio is fixed, then the OCV is shown to decrease with increasing temperature.

Shown in Fig. 6 are the OCV values for Reactions (R3)–(R6), in which the O_2 included in the calculations is assumed to come from atmospheric air ($x_{O_2} = 0.21$). Note that Reaction (R5) gives a lower potential than the direct electrochemical reaction of carbon, Reaction (R3), at temperatures of interest. This is because Reaction (R5) assumes equal activities of CO and CO_2, or a CO/CO_2 ratio of 1. If the CO/CO_2 ratio is in equilibrium in the presence of solid carbon, according to Reaction (R7), the curve denoted by "7" (solid black) is obtained. Equilibrium compositions are calculated with C(s), CO, CO_2, O_2 included in the mixture, with $x \gg 1$. This shows the experimentally proven result that a higher CO mole fraction will produce higher OCVs. Above 1100 K, this curve becomes coincident with the standard potential for C(s) oxidation to CO, signifying that the gas phase is almost entirely CO. Below about 900 K, this curve is coincident with that of Reaction (R3), signifying the gas phase is almost entirely CO_2:

$$xC(s) + O_2 \rightarrow C(s),\ CO,\ CO_2,\ O_2 \quad (R7)$$

$$xC(s) + H_2O \rightarrow C(s),\ CO,\ CO_2,\ O_2,\ H_2,\ H_2O,\ CH_4 \quad (R8)$$

The addition of hydrogen species, as in steam gasification processes, gives a similar result. The standard potential (unit activity) for hydrogen oxidation is shown on Fig. 6. If a H/O ratio of 2 is specified in the presence of excess carbon ($x \gg 1$), a unique equilibrium

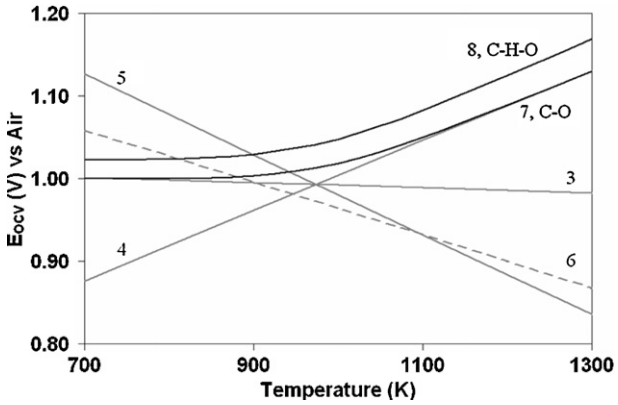

Fig. 6. Theoretical potentials for Reactions (R3)–(R6) at 1 atm total pressure. Grey lines represent standard potentials (unit activity), while the solid black curves represent equilibrium (with $x \gg 1$).

curve can be created, as shown by the (solid black) curve denoted by "8". Equilibrium composition is determined for products C(s), CO, CO_2, O_2, H_2, H_2O(g), and CH_4. The presence of hydrogen can increase the equilibrium OCV over that of the dry C–O system by 20–40 mV as demonstrated in Fig. 6. Note that the OCV is now a mixed potential as there is more than one potential anodic reaction, but in equilibrium the oxygen activity is still fixed.

This result demonstrates that the performance of the gasification driven fuel cell is highly dependent upon the gaseous atmosphere at the anode. The direct presence of the solid char near the anode works to increase the CO/CO_2 ratio and thus cell potential, compared to systems without solid carbon present where the CO/CO_2 ratio monotonically decreases along the anode. The relative magnitudes of the current versus gasification kinetics and bed transport ultimately determine the steady state gas composition.

The open circuit voltages of gasification driven cells were verified experimentally for both the C–O and C–H–O (H/O = 2) systems as shown in Fig. 7a and b, respectively. For these experiments, a commercially available, closed-end, partially stabilized zirconia (PSZ) electrolyte tube was employed. The tube was painted with platinum ink and fired at 1173 K to form porous electrodes, before the tube assembly was immersed in a bed of carbon particles. The data presented in Fig. 7 were taken during temperature ramps between nominally 773 and 1253 K. The ramp rates, in units of K min^{-1}, are given numerically in the legend of the figure. Air was supplied to the cathode on the interior surface of the PSZ tube to maintain a constant oxygen activity. This experimental configuration is identical to that used in previous studies [12,13], and provides a direct means of measuring the effective oxygen activity at the DCFC anode. The PSZ tube is mechanically resilient, allowing for a larger range of heating and cooling rates.

The OCV data for the C–O system is not strongly dependent on heating rate in the range investigated for this configuration. This is likely due to the large thermal inertia of carbon particles in the bed, which would exhibit a time lag. The interior of particles, where most of the active surface area resides, would influence the gas phase composition in accordance with the actual interior surface temperature.

During the cooling ramps, the experimental data with the carbon bed followed the equilibrium curves until the temperature decreased sufficiently to slow the chemical reaction rates in the bed (near 1100 K at these ramp rates). The increase in OCV during cooling below about 1100 K is due to effective freezing of the gas phase composition, which causes the OCV to change slope in accordance with a fixed CO/CO_2 ratio. During cooling to temperatures below 900 K, the OCV decreases with decreasing temperature. This is likely due to the reverse Boudouard reaction, given by Reaction (R1), on the Pt anode since CO_2 and C(s) are thermodynamically preferred at lower temperature (see Fig. 4).

Open circuit potential data for an equimolar CO/CO_2 mixture ($CO/CO_2 = 1$), with no carbon bed, is included with curve "5" in Fig. 7a for comparison. The data for this gas mixture matches with theoretical calculations above 900 K, depicting a scenario with frozen chemical composition (i.e. a forced CO/CO_2 ratio). At lower temperatures, the reverse Boudouard reaction is thermodynamically favored for the equimolar mixture of CO and CO_2, without a carbon bed. Thus the composition is no longer fixed, due to chemical reaction at the electrode.

The data presented in Fig. 7b depicts the inclusion of hydrogen species into the model and show qualitatively similar trends to those in Fig. 7a. The OCV data at temperatures above about 1100 K reach equilibrium values shown by the curve denoted "8", in which Reaction (R8) fixes the oxygen activity at the anode. The C–H–O system is encountered in processes employing steam gasification and, as shown by the data presented in Fig. 7b, behaves similarly to the C–O system.

The transient traces of OCV data are shown in Fig. 8 for the C–O system under isothermal conditions. Measurements were taken immediately after purging an equimolar mixture of CO/CO_2 through a carbon bed, thus causing the OCV to tend towards the standard potential. The flow rate was then stopped, and the OCV was recorded as a function of time at specified temperatures (1196 and 1224 K). As expected, the cell potentials tend to their equilibrium values in the presence of excess carbon, with the higher temperature case exhibiting a faster approach. This result also signifies that given sufficient time, the gases within the carbon bed will tend to equilibrium under open circuit conditions.

The results shown in Figs. 7 and 8 agree with previous work for similar carbon bed arrangements [12,13,22]. As the temperature increases, the gasification reaction rates increase and the gas

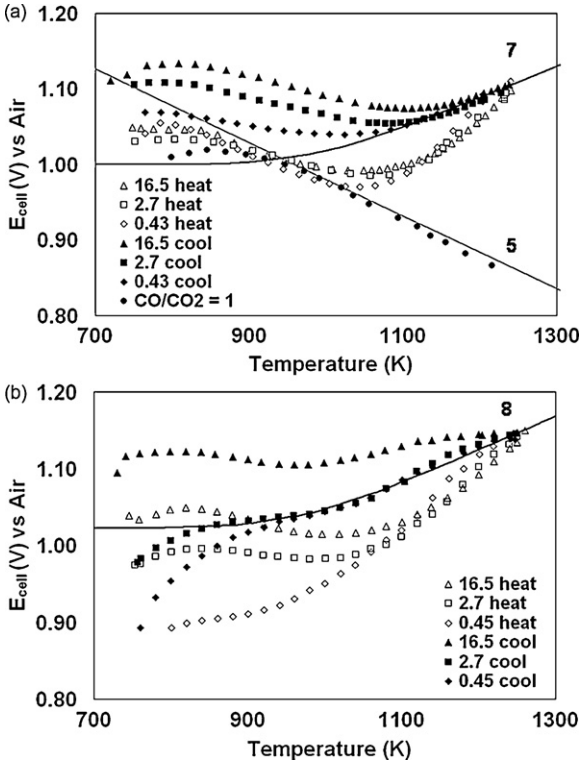

Fig. 7. Comparison of measured cell potentials to theoretical values (Reactions (R5), (R7) and (R8)) for the (a) C–O system and (b) C–H–O system. Open symbols denote heating ramps and filled symbols denote cooling ramps, with the ramp rate (K min^{-1}) given in the figure legend.

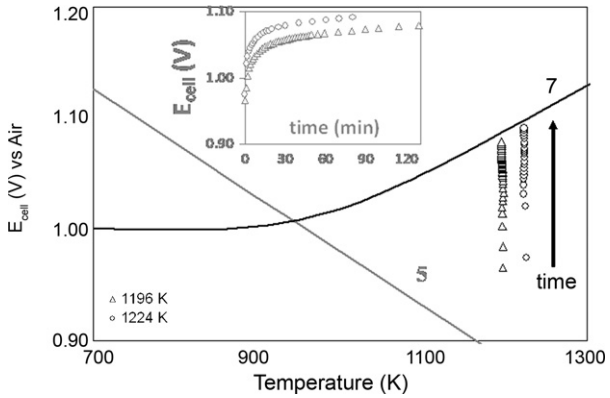

Fig. 8. Transient OCV measurements as the C–O system relaxes to equilibrium at the anode (arrow shows direction of increasing time). Inset shows temporal voltage trace and asymptotic approach to equilibrium.

composition in direct contact with the carbon bed relaxes towards equilibrium.

3. Specific thermodynamic considerations on operational level

The previous thermodynamic and electrochemical analyses show calculable and significant benefit to the direct conversion approach, but neglects any internal irreversibilities inherent to fuel cells as work producers (such as electrode over-potentials, concentration gradients, internal resistances or chemical reactions far removed from equilibrium) or practical operating constraints (such as peak power, utilization and thermochemical driving forces). In order to make a more realistic estimation of the benefit of DCFC over autothermal gasification, systems are analyzed that contain more practical constraints (less than unity air and fuel utilization and specified system temperature) and some irreversibilities such as an operating voltage below the reversible cell potential. Calculations are performed on the basis of 1 kg s^{-1} of solid fuel feed for scale, with all systems operating at a total pressure of 1 atm. Although the efficiency of work producing systems can be cast in a multitude of ways, efficiency here is defined as work output per higher heating value (HHV) of the solid fuel.

The historical coal fired power plant uses a heat engine to extract useful work. Coal and air are introduced to a combustor containing a boiler/superheater, where they are burned to products. The heat release is used to boil an unmixed water stream, and then superheat this stream such that it is suitable for introduction to a steam turbine. The work output and efficiency are dictated by the heat engine used, with the Rankine steam cycle giving a typical thermal efficiency in the range 30–35%. This gives a metric with which the following systems can be measured and compared.

3.1. DCFC plant

The DCFC plant includes gasification and work extraction steps that are mechanically and physically coincident. The gasification process is essentially based on converting solid carbon to gaseous CO by oxygen addition. When the oxygen is added via oxide conducting electrolyte, work and heat are extracted, in contrast to the completely irreversible introduction of gas phase oxygen into the gasifier. This subtle difference allows for higher work outputs as the solid fuel is further converted to CO_2 and H_2O. The DCFC gasifier system does not satisfy the thermal neutral constraint, i.e. is not adiabatic. The fuel utilization, air utilization, and operating voltage are specified in this model study. All internal irreversibilities, or overpotentials, of the fuel cell are included in the operating voltage being less than the reversible cell potential. No air separation unit is required since the solid-state electrolyte is effectively impermeable to N_2. The air introduced into the SOFC is preheated via counter-flow heat exchanger (HX) with a specified effectiveness. Since the fuel bed reactions are endothermic and the fuel cell assembly rejects energy as heat, there will be an internal adverse temperature gradient ($T_{SOFC} > T_{gas}$), creating a similar practical disadvantage as the indirect gasification method. The DCFC is shown schematically in Fig. 9, and could be configured as a tubular or planar geometry with the anode in direct contact with the fuel bed.

The variables $\dot{Q}_{out,SOFC}$ and $\dot{W}_{out}$ refer to the net heat and work outputs of the SOFC. The DCFC system is constrained such that there is not a unique value of CO_2 inflow, so this stream is arbitrary. The products leaving the SOFC are termed flue gas (similarly for each system), with an associated heating value and work potential. Results are presented without CO_2 addition for simplicity, while addition of CO_2 does not change the work output or efficiency, only the flue gas composition and heating value. Note that some gas flow to the gasifier is generally desired for mechanical agitation to segregate ash, fluidization to enhance mixing, and/or entrained fuel delivery. The DCFC arrangement shown in Fig. 9 is a further constrained example of the system shown in Fig. 1.

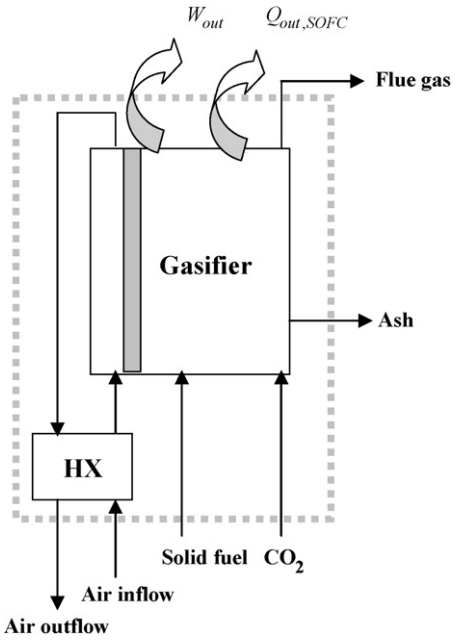

Fig. 9. Schematic of the DCFC plant, with the solid, grey partition denoting the SOFC. Compare the subsystem denoted by the dotted grey line with the control volume in Fig. 1.

3.2. Indirect gasification plant (IDG) with fuel cell

The second system examined is similar to the DCFC plant, except that the gasifier is now physically separate (see Fig. 10). Sensible heat is transferred into the gasifier to drive the endothermic reactions, with the entire process termed indirect gasification. The CO_2 requirement is uniquely determined such that no solid carbon is present in the gasifier effluent. The syngas leaving the gasifier is again converted via SOFC with fuel utilization, air utilization and operating voltage specified. Similar indirect gasification systems,

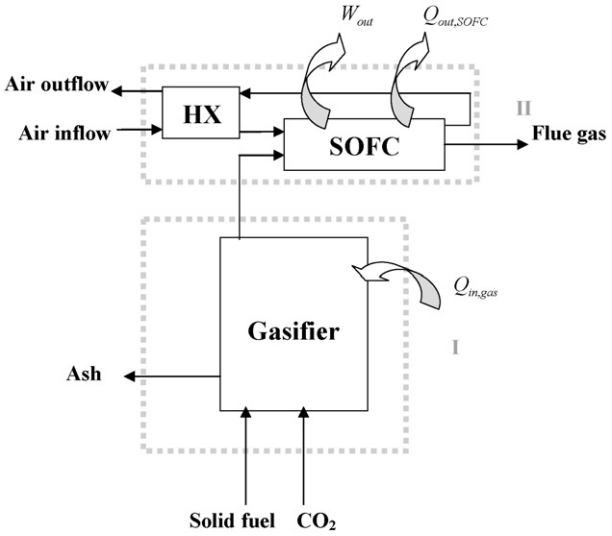

Fig. 10. Simple schematic of the indirect gasification plant. Compare the subsystems denoted by the dotted grey line with the control volumes in Fig. 2.

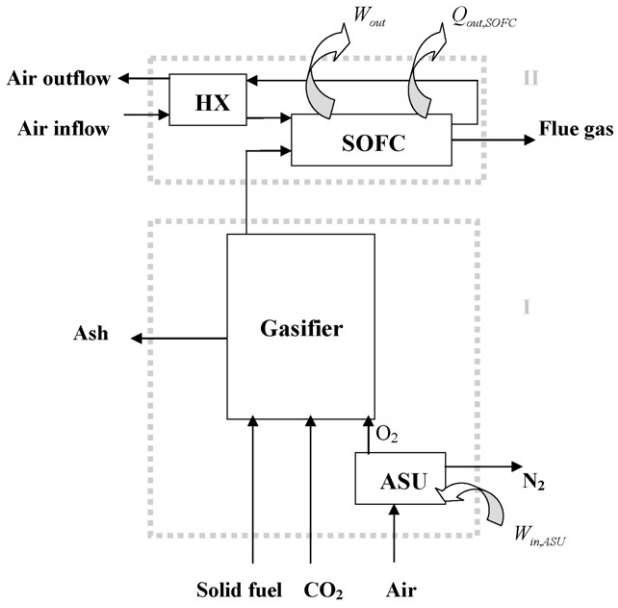

Fig. 11. Simple schematic of the autothermal gasification plant. Compare subsystems I and II denoted by dotted grey lines with the control volumes in Fig. 3.

operating at 1173 K, have been analyzed employing an SOFC as the work producer [23,24]. In that study, heat pipes were used to transfer heat into the endothermic gasifier from combustion of syngas. One concern with the type of arrangement considered here is the source for heat transfer into the gasifier. Reaction of the flue gas with oxygen could supply some heat, as could the fuel cell heat rejection. This trend, although plausible, is opposed to the practical advantage of gasification at higher temperatures (faster reaction rates) and fuel cell operation at lower temperatures (sealing and materials concerns). This isothermal analysis neglects this temperature difference, although alternatives are presented in Section 4.

Again, the variables $\dot{Q}_{out,SOFC}$ and $\dot{W}_{out}$ refer to the net heat and work outputs of the SOFC, while $\dot{Q}_{in,gas}$ refers to heat transfer to the gasifier at 1173 K. The IDG arrangement shown in Fig. 10 is a further constrained example of the system shown in Fig. 2, as denoted by the dotted regions numbered I and II.

3.3. Autothermal gasification (ATG) plant with fuel cell

The plant considered here utilizes O_2 and H_2O, or O_2 and CO_2 to gasify solid fuel under the constraints that no solid carbon is present in equilibrium and the gasifier is adiabatic, operating at 1173 K (see Fig. 11). The scenario using oxygen and steam is similar to the FutureGen process [2,3]. Similar systems have been investigated for coal and biomass utilization with an SOFC as the work producer [25,26]. Note that if carbon dioxide were replaced with water for gasification, results differ by less than 1% in terms of work output, efficiency and oxygen requirements, although gas composition is altered. The syngas is again converted via SOFC with fuel utilization, air utilization and operating voltage specified. An air separation unit (ASU) is included in the analysis since the gasifier is oxy-fired, to prevent dilution of effluent CO_2 by N_2. The work requirement for the ASU is specified as 200 kWh per tonne O_2 (720 kJ $kg_{O_2}^{-1}$), consistent with values reported for cryogenic plants delivering 95% pure oxygen at low pressure [27]. The variables $\dot{Q}_{out,SOFC}$ and $\dot{W}_{out}$ refer to the net heat and work outputs of the SOFC. The gasifier control volume could contain any type of gasifier, although the prevalent technology would be of the circulating fluidized bed type.

The ATG arrangement shown in Fig. 11 is a further constrained example of the system shown in Fig. 3, as denoted by the dotted regions numbered I and II.

3.4. Fuels considered

A range of solid fuels were investigated for each system as shown in Table 1: solid graphitic carbon, several coals, several biomass fuels, and a representative municipal solid waste (MSW). Graphitic carbon is included as a reference solid. The coals selected include Illinois #6 (Ill6) from Macoupin County in Illinois and Wyodak (Wyo) from the Powder River Basin in Wyoming, both of which are included in the Penn State Coal Sample Bank and Database [28] as DECS-24 and DECS-26, respectively. Illinois #6 coal has high-sulfur content while Wyodak coal, on the other hand, has relatively low sulfur content but a large amount of moisture. Switch grass (SG) and almond shells (AS) were selected as representative biomass fuels, although their compositions are similar, and MSW, with high ash and chlorine content, is included as a representative waste fuel [29]. Except for carbon and switch grass, the data presented in Table 1 for the various fuels are on both as-received and dry bases. Significant moisture can be present in the solid fuels, such as Wyodak coal or MSW, which can alter the amount and composition of gases required for gasification. The drop in heating value between as-received and dry fuels is due to the dilatory effect of water, which also reduces the H_2O/CO_2 requirement for gasification. Heating values listed are in units of MJ kg^{-1}.

Any gas cleaning steps are ignored, necessitating that some minor species are present that may be incompatible with current fuel cell anodes. The omission of the gas cleaning step simplifies the comparison, and allows for estimation of impurity levels in the different systems, which is relevant for designing resistant anodes or hot-gas clean-up requirements. All systems would presumably

Table 1
Solid fuel properties used in analysis (wt.%).

Fuel	Volatiles	Fixed C	H_2O	Ash	C	H	O	N	S	Cl	HHV
Carbon[a]	0	100	0	0	100	0	0	0	0	0	32.79
Ill6[b]	35.44	39.74	13.2	11.49	57.33	3.98	8.07	0.99	4.8	0.14	24.55
Ill6 dry[b]	40.83	45.78	0	13.25	66.05	4.59	9.3	1.14	5.53	0.14	28.29
Wyo[b]	33.06	35.06	26.3	5.58	51.42	4.16	11.53	0.69	0.32	0.001	20.82
Wyo dry[b]	44.86	47.57	0	7.57	69.77	5.65	15.64	0.94	0.43	0.001	28.25
AS[c]	70.1	NA	7.8	2.78	46.2	5.5	37	0.68	0.03	0.01	17.55
AS dry[c]	76.1	NA	0	3.07	50.1	5.95	40.1	0.74	0.03	0.011	19.05
MSW[c]	NA	NA	38.5	27.12	18.9	0.6	13.2	0.67	0.48	0.437	7.50
MSW dry[c]	NA	NA	0	44.16	30.8	0.96	21.5	1.09	0.78	0.71	12.20
SG dry[c]	NA	NA	0	10.07	47.8	5.76	35.1	1.17	0.1	0.001	18.02

NA: not available.
[a] HHV from Ref. [20].
[b] Coal properties from Ref. [28].
[c] Biomass and MSW properties from Ref. [29].

require similar gas cleaning technology, although integration into each system would require unique arrangements.

3.5. Model calculations

Chemical reactions are assumed to be in equilibrium for simplicity during the following analysis. This assumption is valid at higher gasification temperatures without significant pyrolysis [30]. Results will be discussed in the context of this assumption. Equilibrium calculations are performed using the element potential method, as described by Reynolds [31]. Species considered in this study for the equilibrium calculations include C(s), CO, CO_2, CH_4, H_2, H_2O(g), COS, H_2S, SO_2, N_2, NH_3, HCl, Cl_2, and O_2.

An energy balance given by Eq. (14) is performed on the gasifier to determine the heat interaction (IDG plant), as well as the input streams (ATG plant). The term $\dot{Q}_{in,gas}$ in Eq. (14) is zero for the ATG and DCFC plants, while the remaining three terms represent the stream enthalpies of the reactants, products, and ash. The ash species considered include solid phase metal oxides. Several fuels considered did not have specific ash composition data available, so for such cases the ash was taken to consist of SiO_2 only. Our calculations indicate that the composition of the ash does not significantly impact values determined for work and energy flows as heat:

$$\dot{H}_r + \dot{Q}_{in,gas} = \dot{H}_p + \dot{H}_a \tag{14}$$

The work output from the fuel cell systems is given by the product of cell operating voltage, E_{cell}, and current, I, as shown in Eq. (15). The current is determined by the oxygen flux, $\dot{N}_O$ in mol s^{-1} (see Eq. (16)), based on a defined fuel utilization value, U_f, of 85%. The fuel utilization of the DCFC plant is defined as the fraction of the supplied oxygen to the total oxygen requirement for full conversion of the carbon and hydrogen in the solid fuel stream to products. In the context of the IDG and ATG plants, the fuel utilization is defined as the percent of the gaseous fuel input to the SOFC that is converted to products. The number of oxygen ions that traverse the electrolyte is given by Eq. (17a) for the GD-DCFC plant, and Eq. (17b) for the IDG and ATG plants. The difference in these two equations arises from the different fuel streams, solid as opposed to syngas, that the SOFC experiences. Note that CH_4 is a minor equilibrium product at 1 atm, and is thus not included. The ATG plant requires an ASU, and this work input must be subtracted from the fuel cell work output to yield the net output. The first law of thermodynamics is then used to determine the heat interaction of the SOFC (see Eq. (18)):

$$\dot{W}_{out,net} = E_{cell} \times I - \dot{W}_{in,ASU} \tag{15}$$

$$I = 2F\dot{N}_O \tag{16}$$

$$\dot{N}_O = U_f(2\dot{N}_{C,fuel} + 0.5\dot{N}_{H,fuel} - \dot{N}_{O,fuel}) \tag{17a}$$

$$\dot{N}_O = U_f(\dot{N}_{CO} + \dot{N}_{H_2}) \tag{17b}$$

$$\dot{H}_r - \dot{Q}_{out,SOFC} = E_{cell} \times I + \dot{H}_p \tag{18}$$

The work output is linearly proportional to the SOFC operating voltage, and there is some practical operating range over which the efficiency and power density will vary.

The air entering the SOFC is preheated to temperature T_{out} in a counter-flow heat exchanger with an effectiveness value, ε, of 0.86. In this analysis, the hot stream always has less heat capacity, $\dot{m}C_P$, due to the removal of oxygen, when determining the cold side air outlet temperature using Eqs. (19) and (20) [32]. In Eqs. (19) and (20), $\dot{H}_i(T)$ represents the enthalpy of stream i, at temperature T, in watts, while the subscripts H and C refer to the hot and cold sides of the heat exchanger, respectively

$$\dot{Q}_{max} = \dot{H}_H(T_{SOFC}) - \dot{H}_H(T_0) \tag{19}$$

$$\dot{H}_C(T_{out}) - \dot{H}_C(T_0) = \varepsilon\dot{Q}_{max} \tag{20}$$

Shown in Eq. (21) is the calculation to determine the air mass flow rate provided for the SOFC where the air utilization, U_a, is defined as the fraction of the oxygen atoms traversing the electrolyte to the total oxygen input from air:

$$\dot{m}_{air} = \frac{I}{4FU_a}(MW_{O_2} + 3.76 \times MW_{N_2}) \tag{21}$$

Stream exergies are calculated using Eq. (22), with the subscript i indicating the steam and subscript 0 indicating the dead state. Mixing of the products with the environment is not considered in this analysis. The exergy of the solid fuel stream is estimated as the heating value [33,34]. A detailed calculation confirms agreement well within 5% for all fuels, assuming that the entropy of the solid is negligible compared to that of the gas streams. The exergies of the flue gas and air exhaust streams, denoted by $\dot{\Psi}_{stream}$, are calculated relative to the products reacted completely to CO_2, SO_2, N_2, Cl_2 and H_2O(L) at 298 K and 1 atm total pressure, with CO_2 exiting as a separate, capture ready stream. The net heat output, $\dot{Q}_{out,net}$, is equal to the heat rejection of the SOFC minus the heat requirement for gasification, as shown in Eq. (23):

$$\dot{\Psi}_{stream} = \sum_{i=1}^{N} \dot{N}_i((h - T_0 s)_i - (h - T_0 s)_0) \tag{22}$$

$$\dot{Q}_{out,net} = \dot{Q}_{out,SOFC} - \dot{Q}_{in,gas} \tag{23}$$

In order to compare different systems, operating on a variety of fuels, several non-dimensional parameters will be formulated. The system efficiency is given by Eq. (24) as the ratio of network output to the heating value of the fuel. The heat rejection (at 1173 K) from the fuel cell, along with the heating value of the flue gas stream can be used in a bottoming process, such as a Rankine cycle. The heating values of the flue gas species contain both the sensible enthalpy change and chemical enthalpy change of complete oxidation to products at 298 K. If the bottoming cycle has an efficiency η_B, then the total system efficiency can be written as shown in Eq. (25):

$$\eta' = \frac{\dot{W}_{out,net}}{\dot{m}_{fuel}HHV_{fuel}} \tag{24}$$

$$\eta'' = \frac{\dot{W}_{out,net} + \eta_B(\dot{Q}_{out,net} + \dot{H}V_{flue})}{\dot{m}_{fuel}HHV_{fuel}} \tag{25}$$

The irreversibility, $T_0\dot{S}_{gen}$ [35], of the gasification and fuel cell process, given by Eq. (26), which along with the system efficiency, gives numerical comparison between the three arrangements:

$$T_0\dot{S}_{gen} = \dot{m}_{fuel}HHV_{fuel} - \dot{W}_{out,net} - \dot{Q}_{out,net}\left(1 - \frac{298}{T_{SOFC}}\right) - \dot{\Psi}_{flue} - \dot{\Psi}_{air,exhaust} \tag{26}$$

4. Results and discussion

The thermodynamic systems analyses are based on the defined parameters given in Table 2. Specifically, the cell voltage is specified at 0.7 V while the air and fuel utilization values are fixed at 20% and 85%, respectively, in agreement with practical operating conditions for SOFCs [2,3,25,26,36,37].

Results for the three fuel cell arrangements are presented in Tables 3–5 on a basis of 1 kg s^{-1} solid fuel input. The DCFC (see Table 3) plant was modeled using fuel data on both the as-received and dry basis for comparison. The raw fuels exhibit lower work outputs than dried fuels due to water dilution, but the thermal efficiencies remain similar to that of raw fuels due to a corresponding drop in HHV. The DCFC is not constrained to require a gasifying agent such as CO_2 or H_2O; the addition of a gasifying agent does

Table 2
Parameters used in systems analyses.

Parameter	Value
ε	0.86
U_a	0.20
U_f	0.85
E_{cell} (V)	0.70
T_{SOFC} (K)	1173
T_{gas} (K)	1173
P_{SOFC} (atm)	1
P_{gas} (atm)	1
η_B	0.30
$w_{in,ASU}$ (kJ $kg_{O_2}^{-1}$)	720

Table 3
DCFC results for various fuels.

Fuel	$\dot{m}_{air}$	$\dot{W}_{out,net}$	$\dot{Q}_{out,net}$	$\dot{H}V_{flue}$	η'	η''	$T_0\dot{S}_{gen}$/HHV
Carbon	49.46	19.14	−2.94	10.27	0.58	0.65	0.17
Ill6	32.65	12.64	−1.11	8.84	0.52	0.61	0.20
Ill6 dry	37.63	14.57	−0.69	9.57	0.52	0.61	0.20
Wyo	29.47	11.37	−2.71	8.39	0.53	0.63	0.22
Wyo dry	39.95	15.43	−2.22	9.93	0.55	0.63	0.20
AS	24.11	9.30	−2.03	7.20	0.53	0.62	0.25
AS dry	26.11	10.08	−1.82	7.45	0.53	0.62	0.25
MSW	7.79	3.01	−0.17	3.67	0.40	0.54	0.30
MSW dry	12.63	4.89	2.34	3.36	0.40	0.54	0.25
SG dry	25.52	9.89	−2.41	7.28	0.55	0.63	0.25

not change the work output or efficiency. However, the addition of CO_2 or H_2O alters the energy transfer as heat, along with the composition of the flue gas. Dried solid fuels were used in the IDG (see Table 4) and ATG (see Table 5) plants, with both CO_2 and H_2O included as gasifying agents, although there is little variation in the work output or efficiency between the agents.

The thermal efficiencies of the standalone IDG and DCFC plant are similar ranging from 39% up to 58%, as compared to 33–35% for the ATG plant. Even with the inclusion of a bottoming cycle, the ATG plant exhibits significantly lower efficiencies of around 50%. Conversely, inclusion of a bottoming cycle boosts the IDG and DCFC efficiencies to nominally over 60%. Quantitatively, if the operating voltage were increased to between 0.75 and 0.80 V, the work output (and efficiency) of the standalone units would increase by 7–14%, respectively. The heat output would be reduced accordingly, such that the effect of the bottoming cycle would be lessened or even unnecessary. Operation at a larger cell voltage would allow more efficient operation, but may require larger reactor length scales and/or cell active area for the same work output. The similar performance between the GD-DCFC and IDG plants is due to similar oxygen requirements for both plants, thus each requires the same current at the constrained operating voltage. This conclusion could also be drawn from Reactions (R1) and (R2), showing that the oxygen requirements are the same. The small deviation in work output between the IDG and GD-DCFC plants is due to the slight difference in the definition of fuel utilization between the two plants.

As noted in Tables 3–5, different fuels give greatly varying results in the GD-DCFC and IDG plants. The lowest system efficiencies are consistently achieved with MSW, which has a large ash content and low heating value. Thermodynamically, pure carbon performs better than all of the heterogeneous fuels, while the coals and biomass fuels perform about equally. The reason for carbon's superior performance in the GD-DCFC and IDG plants is that pure carbon has no oxygen content, and thus requires the most oxygen input in the way of electrical current per 1 kg s^{-1} of solid fuel. The ATG plant does not exhibit significant differences in performance for the different fuels.

Aside from work output and efficiency, there are significant differences between the DCFC and IDG plants. The IDG plant requires significant gas input into the gasifier, due to the constraint that no solids can accumulate. Indirect gasification, however, allows for possible hot or warm cleanup, prior to any contaminants reaching the fuel cell anode. The GD-DCFC does not allow for separate gas cleanup, although there may be some in situ mitigation aside from the use of resilient anodes. These arrangements could benefit from *in situ*, high temperature sulfur capture techniques such as metal oxide sorbents or anode barrier layers.

Table 4
IDG results for various fuels with CO_2 and H_2O additions to the gasifier.

Fuel	$\dot{m}_{air}$	$\dot{Q}_{in,gas}$	$\dot{m}_{CO_2}$	$\dot{m}_{H_2O}$	$\dot{W}_{out,net}$	$\dot{Q}_{out,net}$	$\dot{H}V_{flue}$	η'	η''	$T_0\dot{S}_{gen}$/HHV
Carbon	48.54	19.15	3.87	0	19.14	−6.59	14.04	0.58	0.65	0.19
Carbon	47.67	18.97	0	1.53	18.76	−9.22	17.136	0.57	0.64	0.25
Ill6 dry	36.29	11.82	2.29	0	14.34	−3.02	12.32	0.51	0.61	0.22
Ill6 dry	35.67	11.65	0	0.90	14.04	−4.6	14.28	0.50	0.60	0.26
Wyo dry	39.15	13.71	2.26	0	15.37	−4.46	12.33	0.54	0.63	0.23
Wyo dry	38.22	13.52	0	0.89	15.04	−5.98	14.30	0.53	0.62	0.26
AS dry	25.42	8.32	0.80	0	10.00	−2.63	8.43	0.53	0.62	0.27
AS dry	25.42	8.42	0	0.32	9.87	−3.23	9.14	0.52	0.61	0.29
MSW dry	12.31	1.29	0.58	0	4.85	1.76	4.02	0.40	0.54	0.27
MSW dry	12.19	1.27	0	0.23	4.80	1.36	4.48	0.39	0.54	0.31
SG dry	25.01	8.88	0.85	0	9.81	−3.29	8.31	0.55	0.63	0.26
SG dry	24.59	8.79	0	0.34	9.68	−3.87	9.07	0.54	0.62	0.31

Table 5
ATG results for various fuels with CO_2 and H_2O additions to the gasifier.

Fuel	$\dot{m}_{air}$	$\dot{m}_{O_2}$	$\dot{m}_{CO_2}$	$\dot{m}_{H_2O}$	$\dot{W}_{out,net}$	$\dot{Q}_{out,net}$	$\dot{H}V_{flue}$	η'	η''	$T_0\dot{S}_{gen}$/HHV
Carbon	30.81	0.98	1.09	0	11.37	7.91	8.87	0.35	0.50	0.24
Carbon	30.57	0.98	0	0.44	11.38	7.23	9.58	0.35	0.50	0.26
Ill6 dry	25.31	0.61	0.58	0	9.54	5.93	9.15	0.34	0.50	0.25
Ill6 dry	25.31	0.61	0	0.23	9.49	5.49	9.63	0.34	0.50	0.26
Wyo dry	26.09	0.70	0.27	0	9.79	5.95	8.67	0.35	0.50	0.26
Wyo dry	26.11	0.70	0	0.11	9.77	5.70	8.90	0.35	0.50	0.27
AS dry	17.10	0.46	0	0	6.42	3.75	6.35	0.34	0.50	0.31
MSW dry	11.12	0.07	0.40	0	4.32	2.74	3.67	0.35	0.51	0.27
MSW dry	11.01	0.07	0	0.16	4.30	2.46	3.98	0.35	0.51	0.29
SG dry	16.04	0.49	0	0	5.98	3.52	6.11	0.33	0.49	0.31

Table 6
DCFC flue gas compositions (mole fraction) calculated for various fuels.

Fuel	$CO \times 10^1$	$CO_2 \times 10^1$	$H_2 \times 10^2$	$H_2O \times 10^1$	$O_2 \times 10^{15}$	$N_2 \times 10^3$	$NH_3 \times 10^7$	$H_2S \times 10^3$	$COS \times 10^4$	$HCl \times 10^4$
Carbon	3.0	7.0	–	–	0.45	–	–	–	–	–
Ill6	1.4	5.0	6.1	2.8	1.1	4.7	2.3	19	13	5.3
Ill6 dry	1.7	5.3	5.3	2.2	0.83	5.2	2.0	20	20	5.1
Wyo	1.1	4.3	7.6	3.7	1.2	3.1	2.6	1.2	0.56	0.036
Wyo dry	1.7	5.1	6.6	2.6	0.77	3.9	2.3	1.4	1.1	0.033
AS	1.0	4.4	6.9	3.8	1.5	3.5	2.4	0.13	0.059	0.40
AS dry	1.2	4.7	6.7	3.4	1.3	3.7	2.3	0.12	0.067	0.43
MSW	0.41	3.5	5.1	5.5	5.9	5.9	1.9	3.6	0.91	31
MSW dry	1.7	6.6	2.4	1.2	1.2	13	0.94	6.4	14	65
SG dry	1.2	4.6	6.9	3.5	1.3	6.1	3.1	0.43	0.23	0.041

Calculated flue gas compositions for the GD-DCFC exhaust are given in Table 6. The primary components are CO, CO_2, H_2, and H_2O, as expected. The majority of sulfur is bound in H_2S at the conditions specified (120–20,000 ppm depending upon fuel), with levels reaching as high as 2% of the flue gas stream for Illinois #6 coal. Concentrations of a few hundreds of ppm have been shown to effect SOFC performance [38], and research is ongoing for sulfur resistant anode materials [39,40,41]. Chlorine exists mainly as HCl, with concentrations ranging from 3 to 6500 ppm. A study of HCl effects on SOFC performance indicated that as little as 20 ppm can cause degradation [42]. Cell performance was observed to recover, however, with removal of HCl from the syngas. Very little chlorine exists as Cl_2, which has concentrations (not shown) about 10 orders of magnitude lower than HCl. Nitrogen is primarily bound in N_2, with concentrations of ammonia several orders of magnitude lower.

The O_2 concentrations in the GD-DCFC flue gas give OCV values above 0.79 V, as calculated using Eq. (13), signifying that 0.7 V is an achievable operating potential. This voltage also shows that significant chemical reaction with oxygen is still possible, as the molecular oxygen mole fraction is below 1e−14 in the product streams. The flue gas exiting the fuel cell also contains fuel species, which can release further sensible enthalpy by reacting with oxygen, requiring an ASU to prevent N_2 dilution. The work requirement for this oxygen supply amounts to less than 2% of the SOFC work output, since the majority of the oxygen used to convert the fuel traverses the SOFC. The adiabatic combustion temperature from reaction of the hot flue gas with oxygen at 298 K ranges from over 1600 K for wet MSW to over 2000 K for coal and biomass. This sensible enthalpy could be used to contribute heat into the gasifier similar to the approach of Panapoulos et al. [23,24], along with some heat transfer from the fuel cell to the gasifier or gasifier inlet streams. The IDG and DCFC plants would benefit from this approach, although all three systems would require a similar gas cleaning step. Catalytically stabilized combustion could possibly be used for conversion of the flue gas containing large amounts of CO_2 and H_2O.

The optimal approach to GD-DCFC systems may be to bleed a small amount of gaseous oxygen in to the gasifier to create favorable bed-SOFC temperature gradients, balanced by constraining a majority of the oxygen to traverse the SOFC. This approach would also allow for faster burnout of the char, thus decreasing the required time and/or reactor volumes, and help mitigate tar formation. Char reactivity to O_2 is several orders of magnitude higher than that for H_2O or CO_2 near 1173 K [43].

4.1. Experimental verification of GD-DCFC

In order to demonstrate practical viability of the GD-DCFC, DC current–voltage (*I–V*) characteristics (see Fig. 12) were measured using an anode-supported, tubular SOFC (supplied by Materials and Systems Res., Inc. of Salt Lake City, UT). The cell consisted of a closed-end, 12.7 mm OD Ni/YSZ cermet anode (about 800 μm thick), coated with a 10 μm thick YSZ electrolyte layer. A 100 μm thick layer of strontium doped, lanthanum–manganite (LSMO) served as the cathode. The cathode had an active area of 5 cm^2, which was used to determine the current and power densities. The SOFC was bonded to a stainless steel tube for structural support and gas management. Four grams of raw, Fisher Scientific activated carbon were loaded into the tube interior completely covering the anode, extending approximately 10 cm downstream of the active anode region. A low rate of argon purge (15 mL min^{-1}) was introduced above the carbon bed to mitigate leakage. No change in cell potential was observed when the argon flow rate was changed or stopped. The entire DCFC assembly was placed inside a temperature-controlled tube furnace. High-wattage resistors were used in series to serve as external load, and a DC power supply was used to compensate for the current-collecting lead resistance (roughly 0.1 Ω). The lowest resistive load condition, corresponding to the largest current density of 0.32 A cm^{-2} was held for 40 min, with no noticeable change in current or voltage, indicating stable cell performance. The *I–V* behavior shown in Fig. 12 demonstrates that it is possible to achieve power densities of 220 mW cm^{-2} at 0.68 V from this un-optimized cell at 1178 K. The OCV for a carbon bed at 1178 K is 1.1 V, giving a voltage efficiency of 62% at this condition. This result is an encouraging and promising demonstration for the practical prospects of the DCFC approach.

The presence of solid carbon causes the product gas CO_2 leaving the anodic surface to undergo chemical reactions in the bed. Thus any gas composition measurement downstream of the bed is dependent upon the extent of the electrochemical and chemical reactions. Gas chromatography measurements on the bed exhaust for this configuration showed only CO, with CO_2 mole fractions below the detectable limit. This is in accordance with the CO/CO_2 ratio tending to equilibrium (roughly 36:1 at 1173 K) as the carbon bed is traversed. In this freeboard section, the CO/CO_2 ratio would decrease as the anode is traversed under current flowing condi-

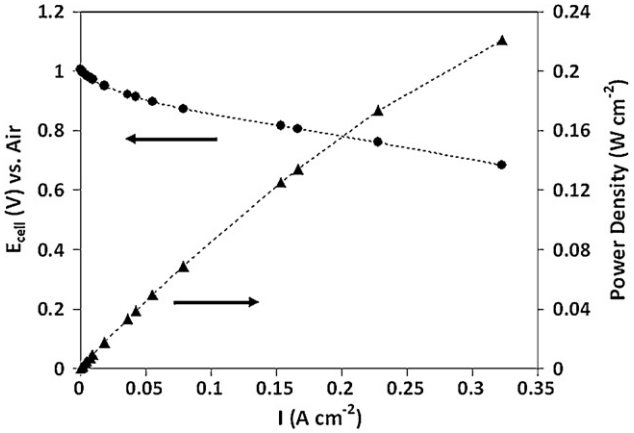

Fig. 12. DC current–voltage measurements for an anode supported GD-DCFC at 1178 K.

tions. Further conversion of CO to CO_2 would require a freeboard section of the GD-DCFC, without solid carbon.

In the absence of carbon, the CO/CO_2 ratio will decrease monotonically as the freeboard section of the anode is traversed under current flow. The decrease in CO/CO_2 ratio will cause a decrease in theoretical cell potential along the anode length in the direction of gas flow. This may necessitate or encourage the use of a separate clean up SOFC, or burner section, rather than attempting to completely convert the gaseous products in the freeboard. This limitation manifests practically in fuel utilizations of less then 100% in the GD-DCFC.

The impact of ash has not yet been addressed in our efforts to characterize direct carbon fuel cells. In our configurations, fresh feed is introduced at the top of the minimally agitated fluidized bed reactor and the operating temperatures of interest are below ash fusion temperatures. Consequently, this arrangement permits dry ash removal from the bottom of the reactor employing conventional ash-handling techniques. Although not within the scope of this study, system scale-up and economic analysis for coal conversion using several DCFC arrangements has been the subject of several recent studies to assess the commercial practicality of the DCFC approach [44–46]. The results of these studies suggest that DCFC technologies are as competitive as pulverized coal and potentially more competitive than advanced coal conversion technologies such as Integrated Gasification Combined Cycle (IGCC) [44,45].

5. Conclusions

Theoretical open circuit voltages were verified experimentally for the gasification driven DCFC system, agreeing with previous findings. Equilibrium compositions are achieved for both the C–O and C–H–O systems with excess carbon at temperatures above 1100 K. Thermodynamic modeling results show that when oxygen is introduced into the fuel stream through a membrane, additional work can be extracted during gasification and conversion. Imposing constraints such as separate gasification steps can lead to lower efficiencies. The GD-DCFC and IDG approaches indicate higher thermal efficiencies than the ATG approach although some practical issues, particularly related to sulfur and other contaminants in coal, must be addressed separately. The efficiency of the gasification driven, solid-state DCFC can achieve over 50% (HHV basis) for a variety of coals, biomass and waste. In addition to high efficiencies, the exhaust stream is CO_2 capture ready, which is a great advantage for sequestration.

In an experimental verification of the GD-DCFC concept under resistive loading, power densities of 220 mW cm^{-2} were achieved at a cell voltage of 0.68 V during operation at 1178 K on a biomass-derived activated carbon. High cell performance and high conversion efficiencies well in excess of 50% reported in this study warrants more attention to solid-state DCFC technology and its practical potential for efficient production of electrical work from carbonaceous solids.

References

[1] J. Deutch, E. Moniz, The Future of Coal—Options for a Carbon-constrained World, MIT Press, Cambridge, MA, 2007, Available at http://web.mit.edu/coal/.
[2] M.C. Williams, J.P. Strakey, W.A. Surdoval, U.S. The, J. Power Sources 143 (2005) 191–196.
[3] M.C. Williams, J.P. Strakey, W.A. Surdoval, J. Power Sources 159 (2006) 1241–1247.
[4] K.R. Williams, An Introduction to Fuel Cells, Elsevier, New York, 1966.
[5] D. Cao, Y. Sun, G. Wang, J. Power Sources 167 (2007) 250–257.
[6] N. Nakagawa, M. Ishida, Ind. Eng. Chem. Res. 27 (1988) 1181–1185.
[7] T.M. Gür, R.A. Huggins, J. Electrochem. Soc. 139 (1992) L95–L97.
[8] B. Wang, D. Zhu, M. Zhan, W. Liu, C. Chen, AIChE J. 53 (2007) 2481–2484.
[9] T. Horita, N. Sakai, T. Kawada, H. Yokokawa, M. Dokiya, J. Electrochem. Soc. 142 (1995) 2621–2624.
[10] M. Ihara, S. Hasegawa, J. Electrochem. Soc. 153 (8) (2006) A1544–A1546.
[11] S. Hasegawa, M. Ihara, J. Electrochem. Soc. 155 (1) (2008) B58–B63.
[12] A.C. Lee, S. Li, R.E. Mitchell, T.M. Gür, Electrochem. Solid-State Lett. 11 (2) (2008) B20–B23.
[13] S. Li, A.C. Lee, R.E. Mitchell, T.M. Gür, Solid State Ionics 179 (2008) 1549–1552.
[14] N.J. Cherepy, R. Krueger, K.J. Fiet, A.F. Jankowski, J. Electrochem. Soc. 152 (1) (2005) A80–A87.
[15] K. Pointon, B. Lakeman, J. Irvine, J. Bradley, S. Jain, J. Power Sources 162 (2006) 750–756.
[16] K. Hemmes, M. Houwing, N. Woudstra, Proceedings of the 3rd International Conference on Fuel Cell Science, Engineering, and Technology, Ypsilanti, MI, USA, May 23–25, 2005, p. 499.
[17] J.F. Cooper, Presented in Direct Carbon Fuel Cell Workshop, NETL, Pittsburgh, PA, USA, July 30, 2003, Proceedings online: http://www.netl.doe.gov/publications/proceedings/03/dcfcw/Cooper.pdf.
[18] S. Zecevic, E.M. Patton, P. Parhami, Carbon 42 (2004) 1983–1993.
[19] T. Tao, Presented in Direct Carbon Fuel Cell Workshop, NETL, Pittsburgh, PA, USA, July 30, 2003, Proceedings online: http://www.netl.doe.gov/publications/proceedings/03/dcfcw/Tao.pdf.
[20] M.W. Chase, J. Phys. Chem. Monogr. 9 (1998).
[21] L. Ma, Combustion and gasification of chars in oxygen and carbon dioxide at elevated pressure, Ph.D. Thesis, Stanford University, Stanford, CA, 2006.
[22] A.C. Lee, R.E. Mitchell, T.M. Gür, AIChE J. 55 (4) (2009) 983–992.
[23] K.D. Panopoulos, L.E. Fryda, J. Karl, S. Poulou, E. Kakaras, J. Power Sources 159 (2006) 570–585.
[24] K.D. Panopoulos, L.E. Fryda, J. Karl, S. Poulou, E. Kakaras, J. Power Sources 159 (2006) 586–594.
[25] A. Verma, A.D. Rao, G.S. Samuelsen, J. Power Sources 158 (2006) 417–427.
[26] Ph. Hofmann, A. Schweiger, L. Fryda, K.D. Panopoulos, U. Hohenwarter, J.D. Bentzen, J.P. Ouweltjes, J. Ahrenfeldt, U. Henriksen, E. Kakaras, J. Power Sources 173 (2007) 357–366.
[27] IPCC, in: B. Meetz, O. Davidson, H.C. de Coninck, M. Loos, L.A. Meyer (Eds.), IPCC Special Report on Carbon Dioxide Capture and Storage. Prepared by Working Group III of the Intergovernmental Panel on Climate Change, Cambridge University Press, Cambridge, New York, NY, 2005.
[28] Penn State Coal Sample Bank and Database, Pennsylvania State University, 2007, Available at http://www.energy.psu.edu/copl/index.html.
[29] Phyllis, Database for Biomass and Waste, Energy Research Centre of the Netherlands, 2007, Available at http://www.ecn.nl/phyllis.
[30] C. Higman, M. van der Burgt, Gasification, second ed., Elsevier, New York, 2008.
[31] W.C. Reynolds, The Element Potential Method for Chemical Equilibrium Analysis: Implementation of the Interactive Program: STANJAN, Version 3.0, Stanford University, 1986.
[32] W.M. Kays, M.E. Crawford, Convective Heat and Mass Transfer, third ed., McGraw Hill, New York, 1993.
[33] V.S. Stepanov, Energy 30 (3) (1995) 235–242.
[34] W.A. Hermann, Energy 31 (2006) 1685–1702.
[35] A. Bejan, Advanced Engineering Thermodynamics, second ed., Wiley–Interscience, New York, 1997.
[36] Y. Yi, A.D. Rao, J.B. Brouwer, G.S. Samuelsen, J. Power Sources 132 (2004) 77–85.
[37] W. Zhang, E. Croiset, P.L. Douglas, M.W. Fowler, E. Entchev, Energy Convers. Manage. 46 (2005) 181–196.
[38] J.P. Trembly, A.I. Marquez, T.R. Ohrn, D.J. Bayless, J. Power Sources 158 (2006) 263–273.
[39] S. Zha, Z. Cheng, M. Liu, Electrochem. Solid-State Lett. 8 (8) (2005) A406–A408.
[40] O.A. Marina, L.R. Pederson, in: J. Huijsmans (Ed.), Proceedings of the Fifth European Solid Oxide Fuel Cell Forum, vol. 1, Lucerne, Switzerland, July 1–5, 2002, p. 481.
[41] H. Kim, J.M. Vohs, R.J. Gorte, Chem. Commun. (2001) 2334–2335.
[42] J.P. Trembly, R.S. Gemmen, D.J. Bayless, J. Power Sources 169 (2007) 347–354.
[43] N.M. Laurendeau, Prog. Energy Combust. Sci. 4 (1978) 221–270.
[44] D. Rastler, Program on Technology Innovation: Systems Assessment of Direct Carbon Fuel Cells Technology, EPRI Report 1016170, April 2008.
[45] T.P. Chen, D. Rastler, Fuel Cell Seminar and Exposition, Phoenix, AZ, October 27–30, 2008.
[46] J. Thijssen, Fuel Cell Seminar and Exposition, Honolulu, HI, November 13–17, 2006.